Scripta Materialia 215 (2022) 114707

Contents lists available at ScienceDirect

Scripta Materialia

journal homepage: www.journals.elsevier.com/scripta-materialia

A predictive model unifying hydrogen enhanced plasticity and decohesion

Meichao Lin [a], Haiyang Yu [*,b], Yu Ding [a], Gang Wang [c], Vigdis Olden [d], Antonio Alvaro [d,e], Jianying He [a], Zhiliang Zhang [a,*]

[a] Department of Structural Engineering, Norwegian University of Science and Technology (NTNU), Trondheim 7491, Norway
[b] Division of Applied Mechanics, Department of Materials Science and Engineering, Uppsala University, Uppsala SE-75121, Sweden
[c] School of Mechanical and Power Engineering, Henan Key Engineering Laboratory for Anti-fatigue Manufacturing Technology, Zhengzhou University, Zhengzhou 450001, China
[d] SINTEF Industry, Trondheim 7456, Norway
[e] Department of Mechanical and Industrial Engineering, Norwegian University of Science and Technology (NTNU), Trondheim 7491, Norway

ARTICLE INFO

Keywords:
Hydrogen embrittlement
complete Gurson model
Hydrogen enhanced plasticity
Hydrogen enhanced decohesion

ABSTRACT

The detrimental effect of hydrogen on metals which manifests itself as a transition from a ductile to a brittle failure mode is, for the first time, incorporated into a unified continuum-scale predictive framework. The complete Gurson model, designed to predict ductile failure by voiding, is extended to include failure by decohesion. Hydrogen enhanced plasticity is accounted for through acceleration of the voiding process while hydrogen induced decohesion is realized by a degradation of the decohesion threshold. The interplay between these two failure modes driven by hydrogen concentration are well captured. This model can predict a realistic level of embrittlement as well as the suppression of dimples in a hydrogen induced fracture surface. Being generic, versatile, and easy to implement, the model may serve as a basis for interpretation of laboratory experiments and enable the transferability of the laboratory results to the integrity assessment of engineering components in hydrogen environment.

Hydrogen embrittlement (HE) is widely foreseen as a challenge in many engineering applications, such as in high-pressure tanks, pipelines, and automotive steels, with respect to the storage, transport, and utilization of hydrogen. Predictive modelling of HE at continuum scale is important for the discovery of hydrogen resistant materials and structural integrity assessment of hydrogen infrastructures. Such model should be able to precisely calculate the hydrogen-induced ductility loss and also represent the characteristic features of the fracture surface morphology. To date, very few available models can satisfy both criteria.

A majority of contemporary studies have confirmed the multifaceted nature of HE as well as various HE mechanisms [1,2], and no single theory can account for all the HE phenomena. In general, many commonly recognized HE mechanisms can be categorized in a dichotomy between the plasticity-mediated mechanisms and decohesion based mechanism. The former category includes the hydrogen-enhanced localized plasticity mechanism (HELP) [3], the hydrogen-enhanced strain-induced vacancy mechanism (HESIV) [4], the adsorption-induced dislocation emission mechanism (AIDE) [5] and the Defactant concept [6,7]. The latter mainly refers to the hydrogen-enhanced decohesion mechanism (HEDE) [8]. Hydrogen enhanced plasticity and decohesion often co-exist in metals [9–16]. Plasticity may act as a prerequisite for final fracture in the form of HEDE [17]. In other cases, hydrogen enhanced plasticity and HEDE compete with each other and its outcome depends on the microstructure [9–12], hydrogen concentration [9,10,13,14], hydrogen trapping [11,15] and the applied loading conditions [9,16]. Naturally arising from the competition is the transition between ductile and brittle fracture mode. For instance, hydrogen enhanced plasticity may dominate at low hydrogen concentrations, giving a so-called quasi-cleavage fracture surface; HEDE may dominate at high hydrogen concentrations leading to completely brittle fracture [9,10,13]. The transition from hydrogen enhanced plasticity to HEDE are also reported in atomistic and meso-scale simulations [18–20].

Being able to model hydrogen enhanced plasticity and HEDE simultaneously and identify the transition between the two are essential but challenging. Most continuum models are based on the preponderance of a single mechanism. The HEDE mechanism has been implemented through cohesive zone modelling (CZM) [21,22] and recently

* Corresponding author at: Norwegian University of Science and Technology: Norges teknisk-naturvitenskapelige universitet, richard birkelans vei 1a, Trondheim 7491, Norway.
E-mail address: zhiliang.zhang@ntnu.no (Z. Zhang).

https://doi.org/10.1016/j.scriptamat.2022.114707
Received 11 January 2022; Received in revised form 13 March 2022; Accepted 24 March 2022
Available online 31 March 2022

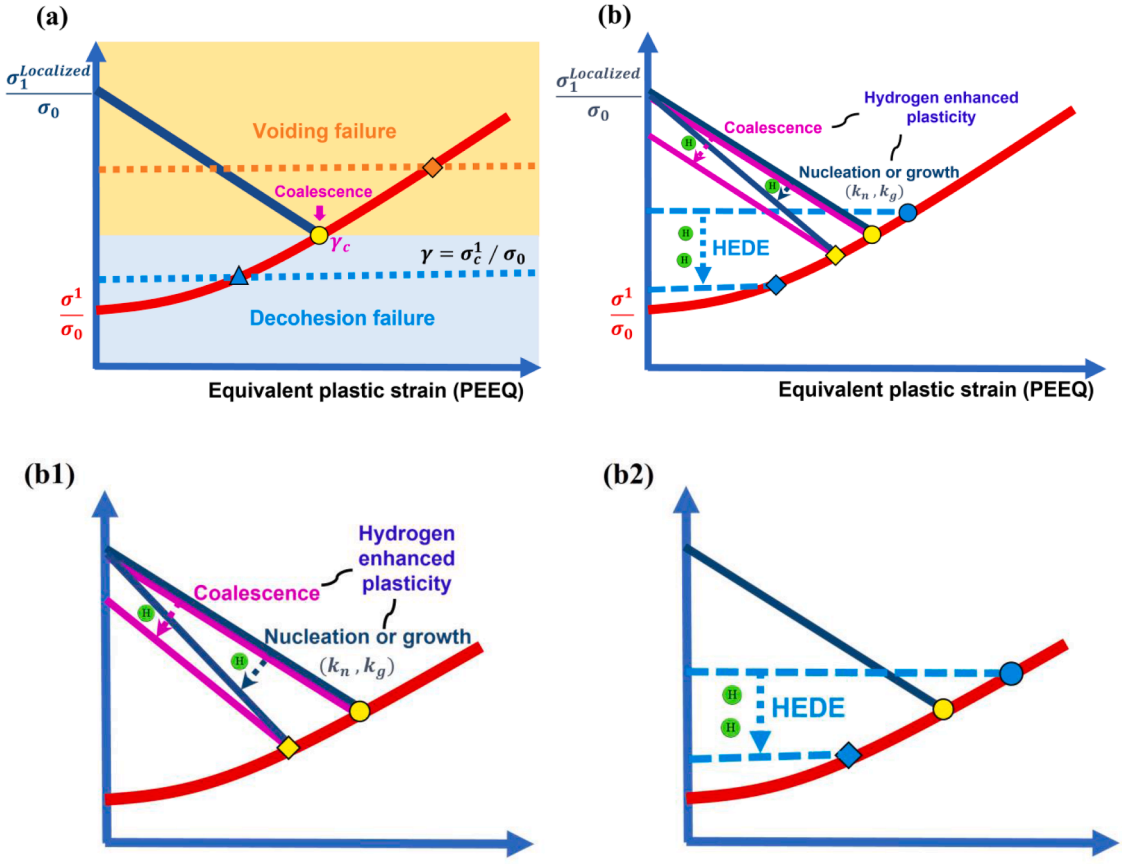

Fig. 1. (a) The schematic of introducing a stress-controlled decohesion criterion to CGM, extending CGM to CGM$^+$; (b) The schematic of hydrogen induced synergistic action of plasticity and decohesion, which is further divided into (b1) hydrogen enhanced plasticity and (b2) HEDE for clarity.

using phase field modelling approach [23]. CZM simulates fracture as an interfacial 'brittle' separation and hence represents brittle fracture features, consistent with many experiments [13,14,24]. The hydrogen dependent cohesive strength can be calibrated using atomistic simulation [25,26] or experiment [27,28]. However, discrepancy arises when interpreting the simulation results in most hydrogen-free scenarios, where the fracture is usually ductile with dimpled morphology [13,14,24,29]. The HELP mechanism has also been used as the basis for continuum-level modelling. The flow stress is described as a decreasing function of hydrogen concentration [30,31]. This exerts an influence on the ductile failure process, e.g. voiding process (micro-void nucleation, growth and coalescence) [30], and shear instability [31]. Recently, Yu et al. [32] proposed a hydrogen informed Gurson model accounting for HELP, where the model parameters were calibrated using a single void containing unit cell approach. Depraetere et al. [33] pointed out that the parameters were too mild to achieve large level of hydrogen 'embrittlement' as observed in a tensile test. They instead proposed empirical hydrogen acceleration functions on either void nucleation, growth, or coalescence, which allowed for a more significant level of 'embrittlement'. However, this treatment [33] reveals that the larger the simulated degree of hydrogen 'embrittlement', the larger the void volume fraction at failure. This contrasts with the experimental evidence which shows that the fracture surface becomes less dimpled as the degree of embrittlement increases, up to a level where fracture surface appears completely brittle [13,24,34]. Obviously, such behavior cannot be captured by the existing hydrogen-Gurson type models (H-CGM) [32,33] where only hydrogen enhanced plasticity is considered.

Triggered by Depraetere et al. [33], we realized that the complete Gurson model (CGM) [35] has a potential to address these challenges. CGM utilizes a plastic limit load model [36] as the criterion for void coalescence.

$$\sigma^1 = \bar{\sigma}\left(\alpha\left(\frac{1}{r}-1\right)^2 + \frac{\beta}{\sqrt{r}}\right)\left(1-\frac{\pi}{4}r^2\right) = \sigma_1^{Localized} \tag{1}$$

The term σ^1 is the applied maximum principal stress in a material with voids assuming homogeneous deformation, while $\sigma_1^{Localized}$ is the threshold for localized deformation mode. r is the void space ratio, α and β are constant. σ^1 and $\sigma_1^{Localized}$ vary with the equivalent plastic strain (PEEQ). In Fig. 1(a), both stresses are normalized by the yield stress of the matrix σ_0. σ^1/σ_0 is expected to increase with PEEQ due to plastic strain hardening, while $\sigma_1^{Localized}/\sigma_0$ decreases with PEEQ because of the evolution of the void. When σ^1/σ_0 intersects with $\sigma_1^{Localized}/\sigma_0$, void coalescence occurs as indicated by the yellow dot. Based on Fig. 1(a), we introduce a stress-controlled decohesion criterion σ_c^1 to denote the threshold for decohesion and integrate it into CGM. For consistency, σ_c^1 is also normalized by σ_0, giving a new parameter $\gamma = \sigma_c^1/\sigma_0$, as illustrated by the dashed lines in Fig. 1(a). In this way, void coalescence and decohesion criteria coexist in CGM, and the new model is referred to as CGM$^+$. The actual failure mode of CGM$^+$ depends on the competition between void coalescence and decohesion. When σ_c^1 or γ is sufficiently large, void coalescence prevails, the 'original' CGM is retrieved, and failure occurs at the yellow dot in Fig. 1(a). If γ is small, decohesion takes charge, and CGM$^+$ fails at the blue triangle in Fig. 1(a). Apparently, there exists a critical value γ_c which signifies the transition from void coalescence to decohesion.

In the model of Depraetere et al. [33] (H-CGM), hydrogen-induced ductility loss was captured by increasing the rate of void nucleation or growth, in accordance with the HESIV [4] or HELP mechanism.

$$\dot{f}_{nucleation}(C) = \dot{f}_{nucleation0}(1 + k_n C) \tag{2}$$

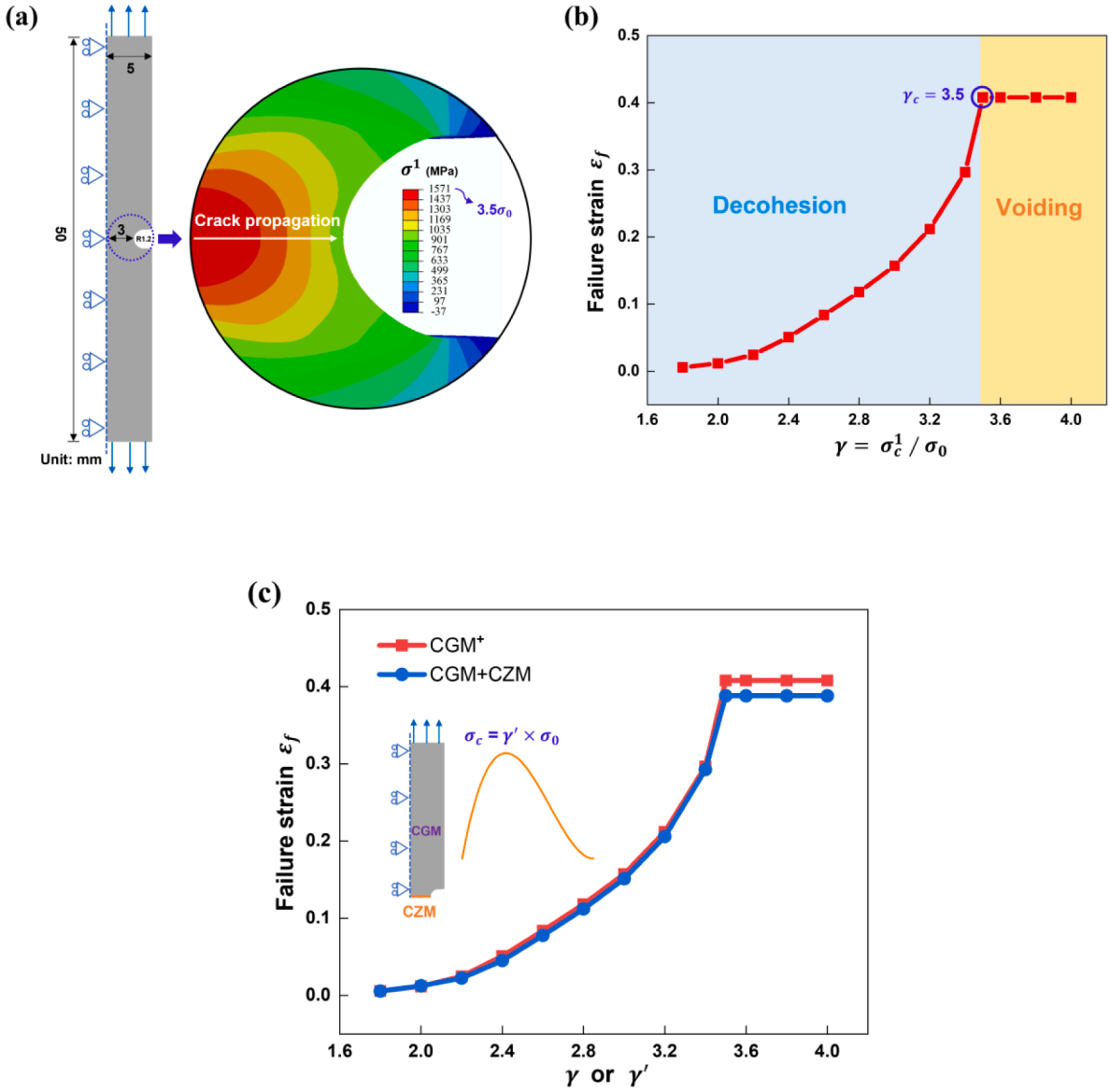

Fig. 2. (a) Geometry of the axisymmetric notched tensile bar specimen, and the distribution of maximum principal stress σ^1 close to the notch root at failure corresponding to $\gamma = 3.6$; (b) The failure strain ε_f versus γ curve, exhibiting a '*S*' shape with an upper plateau and indicating a transition from voiding failure to decohesion failure; (c) The failure strain ε_f versus γ or γ' curves ($\gamma = \gamma'$), comparison of CGM$^+$ and CGM + CZM model, the inset shows the schematic of CGM + CZM model.

$$\dot{f}_{growth}(C) = \dot{f}_{growth0}\left(1 + k_g C\right) \tag{3}$$

where $\dot{f}_{nucleation0}$, $\dot{f}_{growth0}$ are the rates without hydrogen, C is hydrogen concentration and k_n and k_g are hydrogen assisted degradation factors on void nucleation and growth rate, respectively. They also assumed that $\sigma_1^{Localized}$ decreased linearly with hydrogen concentration to account for hydrogen promoted void coalescence [33]. We re-visit H-CGM with a single element simulation and investigate the variation of the $\sigma_1^{Localized}/\sigma_0$ in the presence of hydrogen. The results are schematically illustrated in Fig. 1(b1). The $\sigma_1^{Localized}/\sigma_0$ curve has a sharper slope of decrease (navy blue line) due to hydrogen-increased void nucleation or growth, while it shifts slightly downward (pink line) when considering hydrogen-accelerated void coalescence, both of which make $\sigma_1^{Localized}/\sigma_0$ intersect earlier with σ^1/σ_0, resulting in an earlier failure. It is important to mention that the degree of change in both curves is limited given a realistic combination of hydrogen related parameters, as also noted by Depraetere et al. [33]. This indicates the level of 'embrittlement' simulated by H-CGM is limited, unless exceedingly large hydrogen acceleration is applied.

A hydrogen informed CGM$^+$ model is obtained by allowing the decohesion threshold γ to be degraded by hydrogen, as illustrated in Fig. 1(b2). In this way, hydrogen induced decohesion and hydrogen enhanced voiding are unified in the same model (Fig. 1(b)), which is referred to as H-CGM$^+$. These two failure modes compete and convert from voiding to decohesion when hydrogen concentration reaches a critical value.

The H-CGM$^+$ is implemented using a UMAT[1] subroutine [37] combined with a UMATHT subroutine [38] in ABAQUS. The model geometry is a notch bar, consistent with [33], as shown in Fig. 2(a). The mesh size is 0.1mm × 0.1mm. The same material parameters [33] relevant to

[1] A free copy of the UMAT source code including the decohesion criterion can be obtained from the corresponding author.

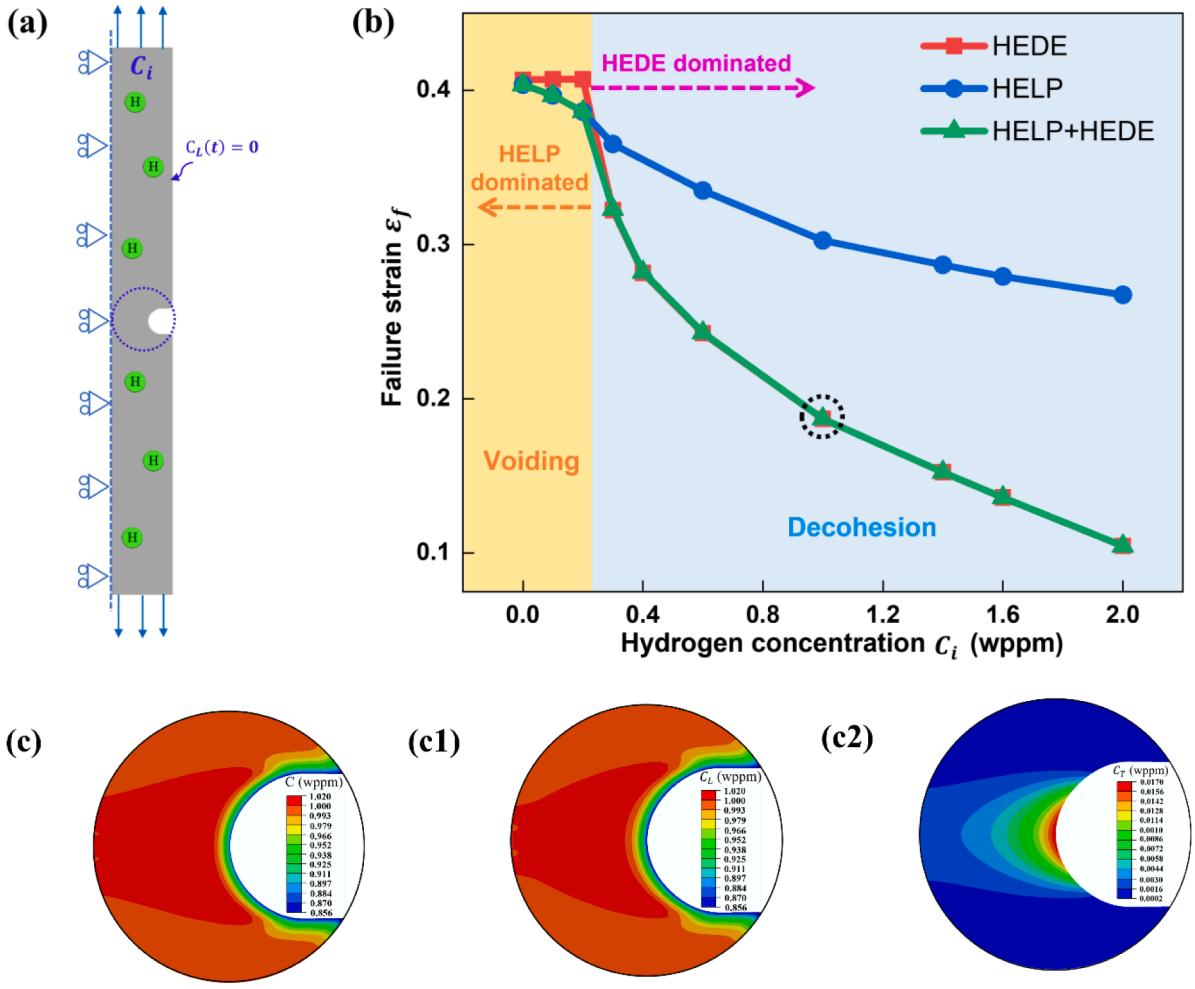

Fig. 3. (a) Illustration of the boundary conditions used in the simulation; (b) The failure strain ε_f versus initial hydrogen concentration C_i curves with HEDE only, HELP only and HEDE + HELP scenarios, respectively; The distribution of (c) total hydrogen concentration C, (c1) lattice hydrogen concentration C_L and (c2) trapped hydrogen concentration C_T at failure corresponding to $C_i = 1$ wppm.

a pipeline steel are applied. All the hydrogen diffusion related equations and parameters are the same as [33]. In the first simulation stage, hydrogen is not considered, and different decohesion thresholds, e.g. γ are examined. The failure strain ε_f of the specimen, calculated based on the radial change of the middle cross section, is plotted against γ, in Fig. 2(b). As γ increases, ε_f rises as expected, and fracture occurs in decohesion mode. When γ reaches a critical value, in this case 3.5, ε_f becomes constant, and fracture occurs by void coalescence. This demonstrates that CGM$^+$ captures a smooth transition from a ductile failure mode to brittle failure mode, which is essential for HE simulation. The critical/transitional normalized decohesion strength $\gamma_c = 3.5$ has a physical meaning. Taking a slightly larger value of γ, e.g. $\gamma = 3.6$, the CGM can be retrieved. At failure, the maximum principal stress σ^1 contour close to the notch root is plotted, in Fig. 2(a). Crack due to void coalescence initiates at site with maximum σ^1, which is 1571 MPa, approximately 3.5 times of σ_0, i.e. $\gamma_c = 3.5$. If the decohesion threshold is smaller than this γ_c, decohesion failure will occur. We continue to show quantitatively that CGM$^+$ is comparable to the CGM+CZM approach, the effectiveness of the latter is established [39]. The same tensile bar is adopted, with the bulk material modelled with CGM and the mid-cross section modelled with CZM. The same material parameters [33] are applied to CGM. A polynomial traction separation law [40] is used for CZM, and different cohesive strengths σ_c are investigated. For comparison, cohesive strength σ_c is also normalized by σ_0, giving $\gamma' = \sigma_c/\sigma_0$. The failure strain ε_f versus γ' curve is plotted against that produced with CGM$^+$, in Fig. 2(c). Good agreement between the two approaches is achieved. The effects of temperature and strain rate on failure mode transition can be considered by implementing a rate and temperature-dependent Gurson formulation [41].

Given the proved equivalence between CGM$^+$ and CZM, the same hydrogen degradation law on cohesive strength in the CZM can be applied to the threshold γ in CGM$^+$. A well-established hydrogen degradation law suitable for pipeline steel is adopted [22] to consider HEDE. The influence of hydrogen on the voiding process is simulated following Depraetere et al. [33] through Eq. (3), in line with HELP. A uniform lattice hydrogen concentration C_i is assigned across the specimen, to mimic the case after hydrogen pre-charging; the hydrogen concentration at the boundary is set to zero upon loading, allowing hydrogen to effuse [33], as given in Fig. 3(a). During tension, hydrogen redistributes according to the stress field, both γ and the void behavior varies in relation to local hydrogen concentration. Simulations with a wide range of C_i are conducted, and the failure strain ε_f is plotted against C_i in Fig. 3(b) (green line). In the absence of hydrogen, fracture occurs by void coalescence; voiding failure dominates also at low hydrogen concentration but occurs earlier (lower strain level), due to hydrogen promoted void growth and coalescence. The failure mode shifts to decohesion when hydrogen concentration is high enough to lower the decohesion threshold, so that decohesion is more favorable, as illustrated in Fig. 1(b). In this case study, the critical hydrogen concentration signifying mode transition is about 0.3 wppm. To

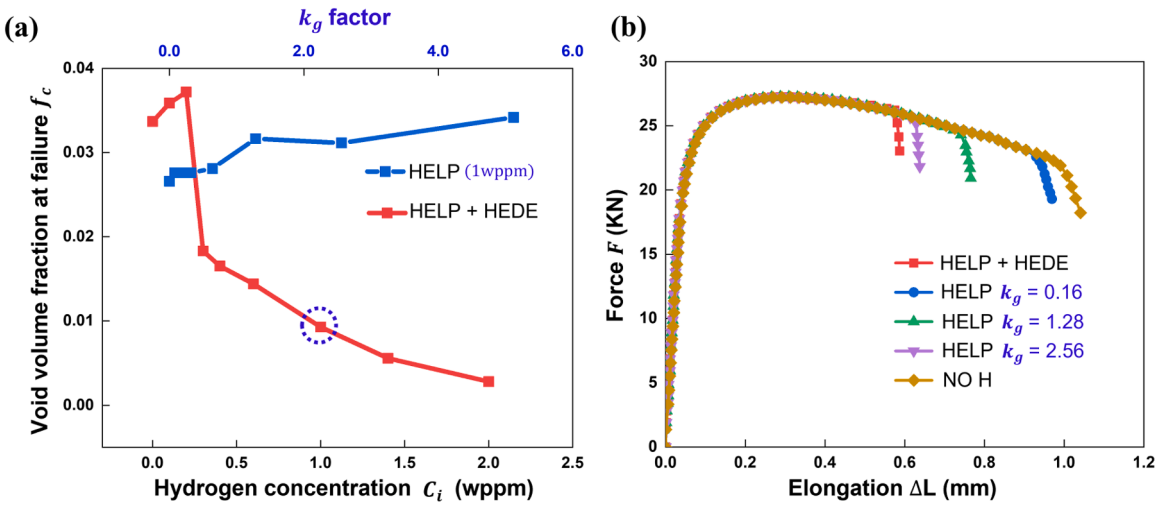

Fig. 4. (a) Void volume fraction at failure f_c versus hydrogen concentration C_i and acceleration parameter k_g investigated in [33]; (b) Force F versus elongation ΔL curves corresponding to $C_i = 1$ wppm, the H-free case is presented as a reference.

demonstrate the competition and transition between the two HE mechanisms, we repeated the simulation with H-CGM$^+$, deactivating void coalescence or decohesion, to represent scenarios only with HEDE or HELP. The failure loci related to these two scenarios are also included in Fig. 3(b). Clearly, the actual failure locus takes the path which leads to earlier fracture. This is a typical result of the competition between different fracture modes - HEDE and HELP in this case. Similar failure loci with a critical hydrogen concentration signifying the failure mode transition were also observed in a few experiments [9,10,13,42]. The distribution of total hydrogen concentration C at failure, partitioned as lattice hydrogen concentration C_L and trapped hydrogen concentration C_T, are shown in Fig. 3(c). C_L and C_T are considered to be in a local equilibrium [43] and preserving mass conservation [44]. Lattice hydrogen dominates in this case, while trapped hydrogen concentrates at the notch root where the largest plastic deformation is. It should be noted that hydrogen-induced fracture may happen in a mixed mode influenced by microstructural features, e.g. HEDE-dominantly at grain boundaries while HELP-dominantly inside grains. We have shown that these can be captured by the H-CGM$^+$ model in the simulation of polycrystals, which will be reported elsewhere.

Let's further compare the fracture loci only with HELP (blue line) and only with HEDE (red line) in Fig. 3 (b). The former has limited ability to realize the significant degree of 'embrittlement' typically observed at high hydrogen concentration. This is because the hydrogen enhanced void coalescence through *inter-ligament necking* is limited, as also pointed out by Yu et al. [32] in unit cell study and Depraetere et al. [33]. To mitigate the problem, one can apply an exceedingly large hydrogen acceleration parameter (Eq (3)) k_g, for example, $k_g = 5.12$ in [33] versus $k_g = 0.16$ calibrated based on unit cell analysis [32]. This treatment, however, implies that hydrogen severely accelerates the growth of voids leading to unrealistic and phenomenologically large void size at fracture surface. This is not in line with most experimental observations where the size of dimples, if existing, is obviously reduced on a highly 'embrittled' fracture surface [13,24,34]. These are the two main issues with the existing H-CGM [32,33] assuming only the HELP mechanism. Fig. 3(b) indicates that the first problem of capturing large loss of ductility is readily solved in the H-CGM$^+$ approach, by implementing also the HEDE mechanism. We subsequently show that this novel approach also gives reasonable prediction of the void size at failure.

In Fig. 4(a), we plot the variation of void volume fraction at failure f_c versus hydrogen concentration C_i. In the HELP dominated area (Fig. 3), f_c slightly increases due to hydrogen promoted voiding. A substantial decrease in the f_c is seen in the HEDE dominated regime. This is consistent with experimental observation in a low-alloyed pipeline steel [13], where the density of dimples on the fracture surface increased with low hydrogen concentrations, while quasi-cleavage fractography with limited dimples was observed at high concentration. The predictions with H-CGM reported by Yu et al. [32] and Depraetere et al. [33] were not able to reflect these observations. Depraetere et al. [33] did systematic simulations adopting different k_g for fixed $C_i = 1$ wppm. For comparison, their results of f_c are also included in the same figure. According to Fig. 3(b), fracture should have occurred in the HEDE mode at the target hydrogen concentration and the f_c is expected to be severely reduced. This cannot, however, be achieved just assuming the HELP mechanism.

To summarize, we have introduced a unified model (H-CGM$^+$) serving for the continuum-level simulation of HE. The HE phenomenon is described within a ductile-to-brittle transition predictive framework where both the hydrogen enhanced plasticity and HEDE are implemented. The model can predict the loss in ductility and the suppression of dimples in a hydrogen induced fracture surface, consistent with most experimental observations. As a practical example, simulation result with H-CGM$^+$ on notched tensile test is presented in Fig. 4(b), showing a good prediction of the HE (red line). The H-CGM$^+$ model is generic, versatile, and easy to implement. It may serve as the basis for the interpretation of laboratory experiments and enable the transferability of laboratory results to in-service integrity assessment of engineering components, such as steel pipelines.

Declaration of Competing Interest

The authors declare that they have no known competing financial interests or personal relationships that could have appeared to influence the work reported in this paper.

Acknowledgements

The authors are grateful for the support provided by Research Council of Norway through the HyLINE (294739) and M-HEAT (294689) projects.

Reference

[1] O. Barrera, D. Bombac, Y. Chen, T.D. Daff, E. Galindo-Nava, P. Gong, D. Haley, R. Horton, I. Katzarov, J.R. Kermode, C. Liverani, M. Stopher, F. Sweeney, J. Mater. Sci. 53 (9) (2018) 6251–6290.
[2] S.K. Dwivedi, M. Vishwakarma, Int. J. Hydrogen Energy 43 (46) (2018) 21603–21616.

[3] H.K. Birnbaum, P. Sofronis, Mater. Sci. Eng.: A 176 (1-2) (1994) 191–202.
[4] M. Nagumo, Mater. Sci. Technol. 20 (8) (2004) 940–950.
[5] S. Lynch, Corros. Rev. 30 (3-4) (2012).
[6] R. Kirchheim, Acta Mater. 55 (15) (2007) 5129–5138.
[7] R. Kirchheim, Acta Mater. 55 (15) (2007) 5139–5148.
[8] R.A. Oriani, Ber. Bunsenges. Phys. Chem. 76 (8) (1972) 848–857.
[9] M.B. Djukic, V. Sijacki Zeravcic, G.M. Bakic, A. Sedmak, B. Rajicic, Eng. Fail. Anal. 58 (2015) 485–498.
[10] M.B. Djukic, G.M. Bakic, V.S. Zeravcic, A. Sedmak, B. Rajicic, Corrosion-Us 72 (7) (2016) 943–961.
[11] M. Koyama, C.C. Tasan, E. Akiyama, K. Tsuzaki, D. Raabe, Acta Mater. 70 (2014) 174–187.
[12] A. Nagao, C.D. Smith, M. Dadfarnia, P. Sofronis, I.M. Robertson, Acta Mater. 60 (13-14) (2012) 5182–5189.
[13] I.M. Dmytrakh, R.L. Leshchak, A.M. Syrotyuk, Int. J. Hydrogen Energy 40 (10) (2015) 4011–4018.
[14] R. Wang, Corros. Sci. 51 (12) (2009) 2803–2810.
[15] W. Krieger, S.V. Merzlikin, A. Bashir, A. Szczepaniak, H. Springer, M. Rohwerder, Acta Mater. 144 (2018) 235–244.
[16] Y. Ogawa, D. Birenis, H. Matsunaga, O. Takakuwa, J. Yamabe, Ø. Prytz, A. Thøgersen, Mater. Sci. Eng.: A 733 (2018) 316–328.
[17] A. Nagao, M. Dadfarnia, B.P. Somerday, P. Sofronis, R.O. Ritchie, J. Mech. Phys. Solids 112 (2018) 403–430.
[18] R. Matsumoto, S. Seki, S. Taketomi, N. Miyazaki, Comput. Mater. Sci. 92 (2014) 362–371.
[19] L. Wan, W.T. Geng, A. Ishii, J.-P. Du, Q. Mei, N. Ishikawa, H. Kimizuka, S. Ogata, Int. J. Plast. 112 (2019) 206–219.
[20] Y. Ding, H. Yu, K. Zhao, M. Lin, S. Xiao, M. Ortiz, J. He, Z. Zhang, Scr. Mater. 204 (2021), 114122.
[21] V. Olden, C. Thaulow, R. Johnsen, E. Østby, Scr. Mater. 57 (7) (2007) 615–618.
[22] L. Jemblie, V. Olden, O.M. Akselsen, Int. J. Hydrogen Energy 42 (16) (2017) 11980–11995.
[23] E. Martínez-Pañeda, A. Golahmar, C.F. Niordson, Comput. Meth. Appl. Mech. Eng. 342 (2018) 742–761.
[24] D. Wan, Y. Deng, A. Barnoush, Scr. Mater. 151 (2018) 24–27.
[25] S. Serebrinsky, E. Carter, M. Ortiz, J. Mech. Phys. Solids 52 (10) (2004) 2403–2430.
[26] D.E. Jiang, E.A. Carter, Acta Mater. 52 (16) (2004) 4801–4807.
[27] H. Yu, J.S. Olsen, A. Alvaro, V. Olden, J. He, Z. Zhang, Eng. Fract. Mech. 157 (2016) 56–71.
[28] N.R. Raykar, S.K. Maiti, R.K. Singh Raman, S. Aryan, Eng. Fract. Mech. 106 (2013) 49–66.
[29] G. Wang, Y. Yan, J. Li, J. Huang, L. Qiao, A.A. Volinsky, Mater. Sci. Eng.: A 586 (2013) 142–148.
[30] H. Yu, J.S. Olsen, J. He, Z. Zhang, Int. J. Hydrogen Energy 43 (21) (2018) 10104–10128.
[31] D. Ahn, P. Sofronis, R. Doddsjr, Int. J. Hydrogen Energy 32 (16) (2007) 3734–3742.
[32] H. Yu, J.S. Olsen, A. Alvaro, L. Qiao, J. He, Z. Zhang, Eng. Fract. Mech. 217 (2019), 106542.
[33] R. Depraetere, W. De Waele, S. Hertelé, Comput. Mater. Sci. 200 (2021).
[34] M.B. Djukic, G.M. Bakic, V. Sijacki Zeravcic, A. Sedmak, B. Rajicic, Eng. Fract. Mech. 216 (2019), 106528.
[35] Z.L. Zhang, C. Thaulow, J. Ødegård, Eng. Fract. Mech. 67 (2) (2000) 155–168.
[36] P.F. Thomason, Acta Metall. 33 (6) (1985) 1079–1085.
[37] Z.L. Zhang, Comput. Meth. Appl. Mech. Eng. 121 (1-4) (1995) 29–44.
[38] R. Fernández-Sousa, C. Betegón, E. Martínez-Pañeda, Acta Mater. 199 (2020) 253–263.
[39] G. Hütter, T. Linse, S. Roth, U. Mühlich, M. Kuna, Int. J. Fract. 185 (1-2) (2014) 129–153.
[40] A. Needleman, J. Appl. Mech. 54 (3) (1987) 525–531.
[41] S. Hao, W. Brocks, Comput. Mech. 20 (1) (1997) 34–40.
[42] A. Shibata, T. Yonemura, Y. Momotani, M.-H. Park, S. Takagi, Y. Madi, J. Besson, N. Tsuji, Acta Mater. 210 (2021), 116828.
[43] R.A. Oriani, Acta Metall. 18 (1) (1970) 147–157.
[44] P. Sofronis, R. McMeeking, J. Mech. Phys. Solids 37 (1989) 317–350.